Thermally Constrained Motor Operation for a Climbing Robot

Salomon Trujillo and Mark Cutkosky
Center for Design Research
Stanford University
Stanford, CA 94305–2232, USA
Email: sjtrujil@stanford.edu

Abstract— **Climbing robots are especially susceptible to thermal overload during normal operation, due to the need to oppose gravity and to frequently apply internal forces for clinging. As an alternative to setting conservative limits on the motor peak and average current, we investigate methods for measuring motor temperatures, predicting motor thermal conditions and generating thermally constrained behavior. A thermal model, verified using empirical data, predicts the motor's winding temperature based on measured case temperature and input current. We also present a control strategy that maximizes robot velocity while satisfying a constraint on the maximum permissible motor winding temperature.**

I. INTRODUCTION

Climbing robots are hard on motors. In comparison to robots that walk or run over the ground, climbing robots have higher average power requirements due to the need to propel the body vertically in opposition to gravity. In addition, they typically apply significant internal forces between opposing limbs to maintain a grip on the climbing surface and prevent slippage. At the same time, the motors used in these robots should be as light as possible, to help reduce the total weight. These requirements conspire to make motor failure an ever-present danger when robots attempt to climb rapidly.

To combat this danger, a partial solution is to use parallel kinematic chains for the legs and/or power transmission systems with differentials, so that more than one motor can contribute to the required torque for each degree of freedom [1]. Even so, the motors are in danger of being overloaded at increased speed or when a strong grip force is required, for example, to scale a tree or a telephone pole.

The primary failure mode of motor overload is overheating of the windings. Commonly, maximum values are set for the short term and continuous torque to avoid damaging the motor. The alternative approach taken in this paper is to construct an empirically validated thermal model of the motors and to use this model in a control scheme that seeks to maximize the vertical speed while keeping the motor windings below the maximum permissible temperature.

Using a commercial low-inertia DC servo motor with a basket-wound rotor (commonly used in robots and haptic interfaces), we describe the motor thermal model and present empirical calibration data. We then consider how to specify the desired torque profile and gait with such motors in the context of a climbing robot. The robot chosen for this work is a variant of the RiSE robot [1] shown in Fig. 1, which has been configured with four legs instead of the
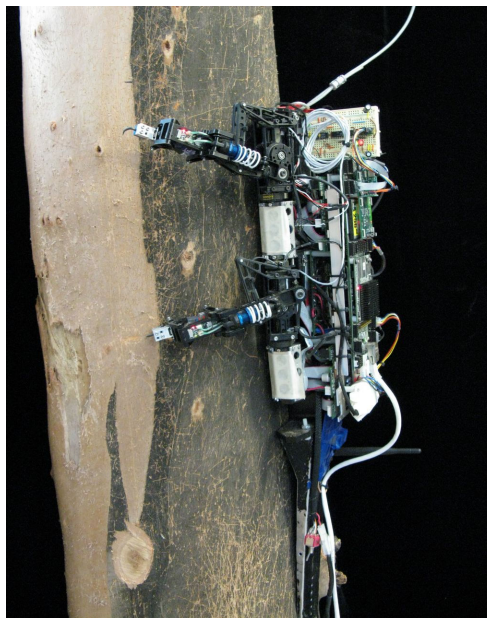

Fig. 1. Four-legged variant of the RiSE robot climbing a tree. The front legs are in swing while the rear legs are in two-legged stance.

usual six. Each leg has two degrees of freedom, driven by a pair of motors through a differential. Passive compliance and damping in each leg help to distribute the forces when the legs are gripping. In comparison to the conventional approach of specifying a limiting peak and average torque, the explicit thermal control scheme permits faster climbing without damaging the motors.

II. TEMPERATURE MEASUREMENT AND PREDICTION

For a basket-wound coreless DC motor, the most likely thermal failure point is the thin wire used for the rotor windings [2]. Thus, in order to drive the motor to its thermal limits, a measurement or accurate estimate of the winding temperature is required. This section presents a thermal model that can estimate the winding temperature in short- and long-term operation as well as the measurement method used to verify the model.

A. Thermal Model of the Motor

We predict the winding temperature using a simple lumped parameter thermal model, shown in Fig. 2, a method often
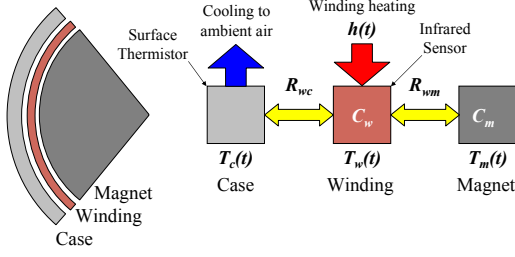
Fig. 2. Left: quartered cross-section of a coreless basket-wound motor. (Not to scale) Right: Block diagram for lumped parameter thermal model of motor. (Definitions of symbols are given in the text.)

Fig. 3. Diagram of experimental setup showing motor, sensors and applied load.

used for electric motors [3][4][5][6]. For basket-wound motors, we model the outer case, the motor windings and the inner magnetic stator. The model is given by the system of equations:

$$C_w \frac{dT_w(t)}{dt} = \frac{T_c(t) - T_w(t)}{R_{wc}} + \frac{T_m(t) - T_w(t)}{R_{wm}} + h(t) \quad (1)$$

$$C_m \frac{dT_m(t)}{dt} = \frac{T_w(t) - T_m(t)}{R_{wm}} \quad (2)$$

where t is time, and $T_w(t)$, $T_c(t)$ and $T_m(t)$ are the temperatures of the motor winding, the outer casing and the magnetic stator respectively. The unknown parameters in this model are the winding's heat capacity (C_w), the magnetic stator's heat capacity (C_m), the thermal resistance between the windings and the outer casing (R_{wc}) and the thermal resistance between the windings and the magnetic stator (R_{wm}).

The Joule heating of the motor windings is given by $h(t)$ which is expressed as

$$h(t) = I(t)^2 R \left(1 + \alpha(T_w(t) - T_0)\right) \quad (3)$$

where $I(t)$ is the current passed through the motor coil and R is the resistance of the motor coil at $T_0 = 25°C$. α represents the temperature coefficient of resistance, which for copper is 6.8×10^{-4} [7]. Basket-wound coreless motors do not generate heat via iron losses [2].

Heat dissipation from the motor housing can be difficult to model because it involves determining the convective transfer to the ambient air and conductive transfer through the motor mounts, both of which are dependent on environmental temperatures [8] and motor mounting. Rather than attempting to predict the outer case temperature ($T_c(t)$), we measure it directly with a surface thermistor.

B. Temperature Sensors

To verify and calibrate our thermal model we conducted tests on a 110182 Maxon A-Max motor (7 watt rating, 26 mm case diameter, 117 gram mass) [9]. This motor has a low winding resistance of 0.54 ohms. A non-contact sensor is required for direct measurement of the motor windings to prevent any physical interference during motor operation. The experimental setup is depicted in Fig. 3. Measuring temperature via changes in rotor resistance has been used for thermal monitoring in AC motors [10], but cannot be used
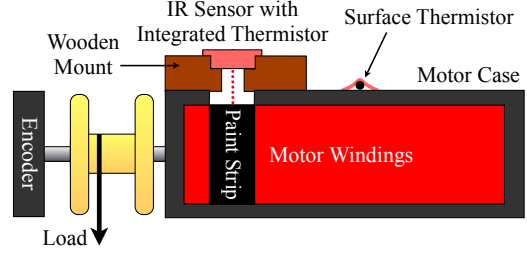
for a small brushed motor *in situ* because of the varying resistance due to commutation.

For the non-contact sensor, we cut a small opening in the outer casing of the motor and mounted a Smartec SMTIR9902 infrared sensor in an insulating mount very close to the surface of the rotor. Wood was chosen to provide thermal insulation from the motor casing. Since thermopile infrared sensors measure a temperature differential between the sensor and the target surface, the infrared sensor has an integrated thermistor used to determine the base sensor temperature [11]. Further, because the emissivity of the copper windings is low (approximately 0.2), a thin layer of black paint, with an emissivity around 0.98, is applied to the motor windings which increases the signal to noise ratio of the infrared readings.

The infrared sensor was calibrated using a bare motor rotor that had been removed from its casing and disconnected from the commutator. The resistance of the copper is linearly-dependent on temperature over the motor's operating range and can be used as a ground truth for calibration. The resistance was measured using a Kelvin four-wire method [11] with a sensing current of 3 amperes. The high-current sensing signal increases the signal-to-noise ratio at the expense of inducing internal heating. To mitigate this effect, the resistance is only measured every 100 milliseconds using a single 1ms burst of current. The calibration of the sensor was found to be accurate to within $\pm 0.3°C$ due to discretization and within $\pm 1.5°C$ due to daily sensor drift.

In order to measure the temperature of the motor casing, we employed an Omega Engineering SA1-TH series 2.2K ohm surface-mount thermistor, which adheres directly to the motor casing for good thermal conductivity and fast response. We linearized the output of the sensor by connecting it in series with a 400 ohm resistor [12] whose value was determined empirically.

C. Experimental validation of thermal model

The winding's heat capacity can be determined by measuring the rate of change of winding temperature during the initial heating of the motor. If the entire motor is initially at thermal equilibrium at $t = 0$, then (1) reduces to

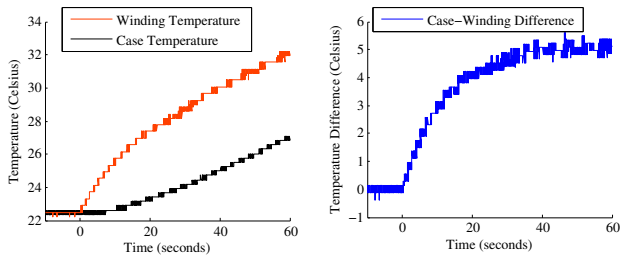$$C_w = \lim_{t \to 0} \frac{h(t)}{dT_w(t)/dt} \quad (4)$$

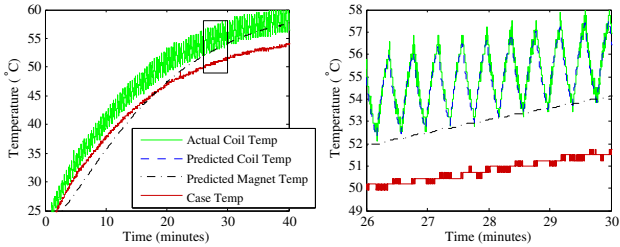Fig. 4.   Typical thermal step response at 3.9A

Fig. 5.   Simulated and actual motor temperatures for a 24 s period square-wave at 0-3.8 A. "'Predicted Coil Temp'" is omitted on the left for clarity, as it is indistinguishable from the actual temperature. Plot at right is a magnified view of the boxed area on the left.

The thermal resistance between the windings and the outer case can be determined by examining the temperature difference during constant heating once the system reaches thermal steady-state:

$$R_{wc} = \lim_{t \to \infty} \frac{T_w(t) - T_c(t)}{h(t)} \qquad (5)$$

As shown in Fig. 4, the windings have a time constant of 12 seconds given by the 63% rise time of $T_w(t) - T_c(t)$, which is relatively slow when compared to the period of climbing gaits, but fast when compared with the outer casing thermal time constant. The thermal parameters of the magnetic stator must be inferred since we are not directly measuring its temperature.

D. Determination of Remaining Thermal Parameters

Using a simulation of the thermal model, we fit the thermal parameters to empirical data through a random searching of the parameter space. To train the thermal model, the motor is mechanically constrained and excited using a 0–3.8 ampere square-wave current with a period of 24 seconds. (If a single current step is delivered, parameter estimation will favor the slow magnetic rotor response, sacrificing the fit of the fast winding response.) A typical fit to training data is shown

TABLE I

THERMAL PARAMETERS

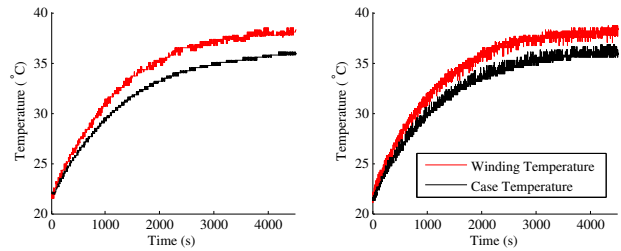| Winding-Case Thermal Resistance	1.1 K/W
windings Heat Capacity	13 J/K
Winding-Magnet Thermal Resistance	2.9 K/W
Magnet Heat Capacity	68 J/K

Fig. 6.   Left: 1.3W motor heating from a constant 1.54A current. Right: 1.3W motor heating from a 50% duty-cycle 1.00-1.95A square-wave current.

in Fig. 5 and the results of the parameter fit are provided in Table I. When these parameters are compared against several other test datasets, we find the RMS of the error between winding temperature and predicted winding temperature is 1.75°C, which is comparable to the drift error of the sensors.

E. Heat Transfer under Static vs. Dynamic Conditions

In order to apply the simple thermal model to a robotic system with complex motor trajectories, the model cannot be dependent upon rotor speed. The motor has a 0.5 mm air gap between the windings and the outer case, which is considered small enough to make convective transfer negligible under stationary conditions [13]. Under non-stationary conditions, the motor will be spinning up to 20 rad/s; thus, for a 10 mm radius, the mean air speed in the gap will reach upwards of 0.1 m/s. For an air kinematic viscosity of air at 80°C at 2.12 m²/s, the Reynolds number for a 0.5 mm gap is around 2.3, which is well below turbulent flow, preventing forced convective heat transfer.

We empirically verified these claims by comparing two scenarios shown in Fig. 6: static heating where the rotor is fixed and dynamic heating where the motor is free to spin. For the dynamic case, we loaded the motor by attaching a 200 gram weight via a 6 mm diameter pulley directly to the motor shaft. We applied a 50%-duty-cycle square-wave current source to the motor, with the high current at 1.95 A and the low current at 1.00 A. Applying (3) and averaging, this square wave produces a mean heating power of 1.3 W. For the static case, we use (3) to calculate that a constant 1.54 A current will produce equal thermal power.

The heating curves from Fig. 6 show that the static and dynamic cases are nearly identical. The difference between the two sets is ±1°C, which is well within the noise of the sensors. The increased noise of the dynamic test is attributed to the increased electrical noise produced by brush commutation.

III.   CLIMBING BEHAVIOR UNDER THERMAL CONSTRAINTS

We base our climbing strategies on a version of the multi-purpose climbing and walking RiSE robot configured as a quadruped. Each leg is powered by two RE16 Maxon Motors [14] through a differential gearing system [1]. In this paper we concentrate on strategies for pole and tree climbing. As shown in Fig. 7, each leg is capable of producing a vertical
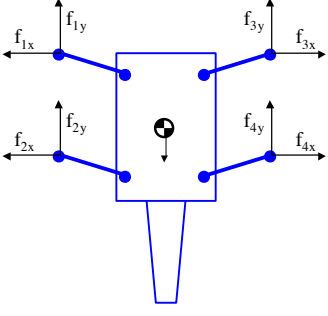
Fig. 7. Schematic of the RiSE robot showing vertical and clamping forces on the legs.
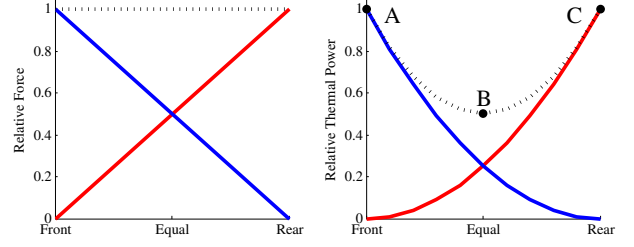

Fig. 8. Left: Normalized distribution of force f/f_{max} Right: Normalized winding heating. P/P_{max} A: Heating during front two-legged stance. B: Optimal heating during four-legged stance. C: Heating during rear two-legged stance.

force f_{iy} to locomote upward and a lateral force f_{ix} used to grip the pole. Based on experience with the robot, we choose a simple, fast and stable bounding gait [15] by specifying that $f_{1y} = f_{3y}$ and $f_{2y} = f_{4y}$ and setting the front and back pair of legs 180° out of phase. The gait stride length is set to the robot's kinematic maximum to reduce the number of attachment and detachment events, each of which carries an energy cost.

The resulting bound gait is implemented by a state machine with the following sequence:

1) A *four-legged stance* in which the robot holds the tree and pulls itself upward with all four legs.
2) The front pair of legs detach and enter *swing* while the rear pair remains in *two-legged stance*.
3) The front pair rapidly swings to a forward position while the rear legs continue to propel the robot upward while the robot's tail provides counterbalance.
4) The front pair reattaches to the tree, both pairs entering *four-legged stance* and the cycle repeats with reversed roles for the upper and lower pairs of legs.

Note that the amount of time spent in two- versus four-legged stance is controllable.

During the detachment, swing and attachment sequence, the robot employs a bang-bang controller constrained by maximum voltage for time-optimal control [16]. During stance phases, the robot's upward velocity is regulated using a PI control law while internal grip forces are maintained using a feedforward voltage command, which maintains an approximately constant normal force during the stance phase for each pair of legs. For the purposes of cataloging data, we consider three different phases: four-legged stance, two-legged stance and swing (which includes detachment and attachment).

A. Thermal Minimization

The torque produced by each DC motor is proportional to the current passed through its windings. [2]

$$M_i(t) = K_\tau I_i(t) - T_{frict} \qquad (6)$$

where $M_i(t)$ is the torque produced by the motor, K_τ is the motor torque constant, T_{frict} represents friction and i indexes the various motors. Since (3) is quadratic, while

(6) is linear, there is a thermally optimal distribution of forces between the legs. For the present case, if we assume a constant scaling between motor torque $M_i(t)$ and vertical force f_{yj} and apply the constraint $f_{1y} + f_{2y} = \frac{mg}{2}$ (where m is the robot mass and g is gravational acceleration) and plot the force and thermal heating distribution as we transfer weight between the two pairs of legs as shown in Fig. 8, we found that the total thermal losses are minimized when the forces are evenly distributed between the front and back feet at point B. Thus, it is desirable for all four legs to be in contact with the climbing surface as long as possible such that the weight can be distributed among as many legs as possible. Points A and C are unavoidable during swing phase, but the duration of the phase is minimized by the bang-bang controller.

Although they are not considered here, different gaits or robot platforms may prevent a thermally ideal force distribution. For example, for robots climbing with directional adhesion [17], it is desirable to bear most of the vertical load on the front feet to maximize adhesion. However, for thermal reasons, it is advantageous to distribute the loading force evenly among the legs. We note also that maximizing the swing phase velocity will always increase the average number of legs in contact independent of the desired gait.

B. RiSE Specific Considerations

The RiSE robot has a differential transmission on each leg that couples two motors, designated as motor "A" and motor "B", using the following transformation:

$$M_{iA} = \frac{1}{2}(n_x f_{ix} + n_y f_{iy})$$
$$M_{iB} = \frac{1}{2}(n_x f_{ix} - n_y f_{iy}) \qquad (7)$$

where n_x and n_y are the respective transmission ratios for the vertical and lateral degrees of freedom. The practical ramification of (7) is that the absolute value of M_{iA} will always be greater than M_{iB} during the more significant stance phases since both f_{ix} and f_{iy} are positive; therefore, we only need to monitor the temperature of the motor "A" on each leg for possible thermal overload.
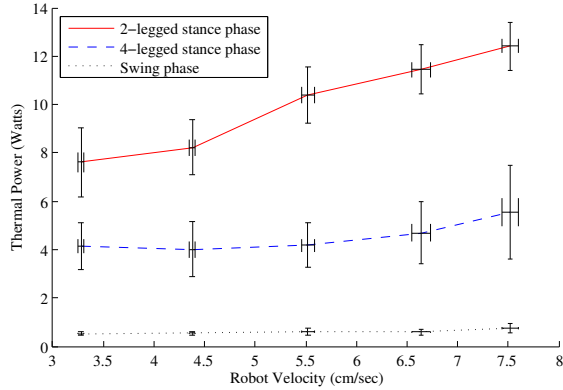
Fig. 9. Average thermal dissipation in a single "A" motor for seperate phases as a function of robot velocity. Error bars indicates the standard deviation in average power between individual gait periods.
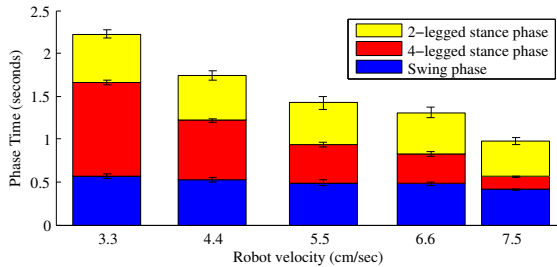

Fig. 11. Average thermal dissipation of a single "A" motor as a function of robot velocity. The data is determined by multiplying the values in Fig. 9 by the percentage of time spent in each phase. Each slice indicates the contribution of each phase to total motor thermal power.

Fig. 10. Gait period as a function of robot velocity. Each slice indicates the division of the gait period between the various phases.

C. Winding Heating as a Function of Velocity

While we expect the thermal power to increase monotonically as a function of robot velocity, we cannot easily construct a theoretical model that accounts for the variations of friction with velocity, loading, etc. Therefore, we determine the winding heating dependence on velocity empirically.

We collected data at five different velocities, using several climbing trials at each velocity. Above the fastest presented velocity, the robot had difficulty producing enough lateral force to prevent slipping without increasing the voltage supply. Below the slowest presented velocities, the legs begin to experience intermittent stiction indicating that a bound gait is not suitable for slow climbing. Thermal power is estimated by measuring the current in the "A" motors and applying (3). Because of the relatively long thermal time constant of the motors, listed as 10.5 seconds [14], variations on the time scale of the gait period will not affect the winding temperature. Fig. 9 shows the average thermal power dissipated during each phase. Note that the error bars represent variability of the average between cycles and not the variation of power within a single cycle.

Since our swing phase velocity is maximized independent of commanded robot velocity, we expect the duration of the swing phase and subsequently the two-legged stance to be a fixed minimum as verified in Fig. 10. As robot velocity increases, the relative contributions of these two
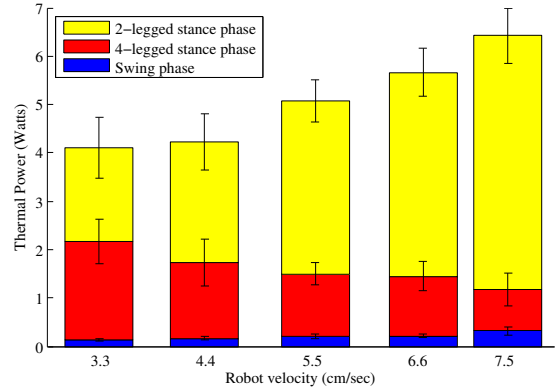
phases increase. By combining the value obtained in Fig. 9 with the percentage of time spent in each phase, derived from Fig. 10, we can calculate the average thermal power dissipated by the robot as shown in Fig. 11.

D. Thermal Regulation

If the robot continually drives at the maximum velocity permitted by thermal constraint, then the winding temperature will be held constant at its allowable maximum. By measuring the motor case temperature and applying (1) we can estimate the amount of heat dissipated by the motor which, in turn, is the maximum permissible thermal power. Due to the thermal mass of the windings, only the average thermal power must match the thermal dissipation as given by

$$\frac{1}{\Delta t} \int_{t_0}^{t_0 + \Delta t} h(t) \, dt \leq \frac{T_{max} - T_c(t)}{R_{wc}} \qquad (8)$$

where t is the current time, Δt is the thermal time constant, t_g is the gait period and T_{max} is the maximum permissible winding temperature minus a safety factor to allow for errors in the sensors and control. Notice that this statement is equivalent to placing an upper bound on the RMS of the motor torque. Equation (8) does not account for the heat capacity of the windings or the magnetic rotor, so a more sophisticated controller would employ an estimator using (1) and (2) in order to get additional speed during the initial heating of these components.

Because the thermal power greatly varies within the gait cycle, attempting to exert control at bandwidths higher than the gait frequency is counter-productive. Thus, at each footfall, the maximum desired velocity is calculated using (8) to find the maximum allowable thermal power for the upcoming gait period. In turn, the maximum velocity can be calculated from the inverse of the data presented in Fig. 11. Because the climbing is performed in an unstructured environment, the actual thermal power generated for any given stride is random. In the event of a power spike, the time constant
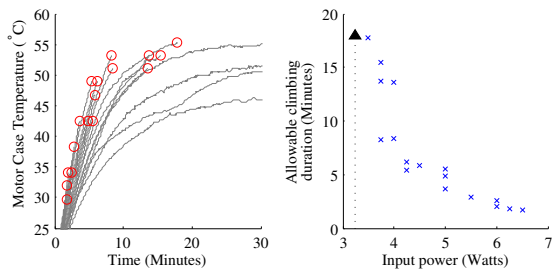
Fig. 12. The allowable time spent at each level of power dissipation. This data was recorded at 17°-20°C using "A" motors mounted on RiSE.

of the windings is long enough that the robot has ample opportunity to reduce speed and dissipate the extra heat.

E. Climbing Duration

As noted in II-E, the motor thermal properties are independent of whether is spinning or stationary. Therefore, tests on a stationary motor exerting torque will yield an estimate of the maximum climbing time subject to thermal constraints. By applying a constant current to provide the power specified by (3), the outer case heats until the constaint given by (8) is violated. These tests essentially indicate the effects of ambient temperature and heat conduction into the robot chassis.

At 17°–20°C ambient temperature, the robot is able to dissipate around 3–3.25 watts indefinitely; however, our slowest presented speed is 3.3 cm/sec which produces 4 watts of heat. As shown in Fig. 12, this speed allows for approximately 8–12 minutes of climbing. At the maximum tested speed in Figs. 9-11, the robot produces 6.4 watts and could climb for around 2 minutes before having to reduce speed.

IV. CONCLUSIONS

We have described an approach to regulating the temperature of direct current motors for a vertically climbing robot based on predictions from a thermal model. To empirically validate the simple lumped-parameter thermal model, we first conducted experiments on an isolated motor using a non-contact infrared temperature measurement of the windings and a surface-mount thermistor on the motor case. We established that by measuring the input current and motor case temperature, winding temperature can be estimated independent of changing ambient conditions.

We then explored the effects of a symmetric bounding climbing gait on the thermal capacity of the motor. Heat dissipation is reduced when forces are distributed among several actuators, suggesting that the duration of the non-contact swing phases should be minimized. However, since the swing phase has a minimum duration constrained by system friction and available supply voltage, increasing robot velocity has the effect of decreasing the average number of legs in contact and thus increases motor heating.

Initially, the maximum velocity is thermally unconstrained as the motor windings are not at their maximum permissible

temperature. Once the temperature limit is reached (after a few minutes in the case of the RiSE robot) climbing velocity is restricted such that the heat dissipated by the windings equals the mean heat generated. Thus, our method allows a robot to use the initially available thermal capacity for faster climbing.

V. ACKNOWLEDGEMENTS

REFERENCES

[1] M. J. Spenko, G. C. Haynes, J. A. Saunders, M. R. Cutkosky, A. A. Rizzi, R. J. Full, and D. E. Koditschek, "Biologically inspired climbing with a hexapedal robot," *J. Field Robot.*, vol. 25, no. 4-5, pp. 223 – 242, 2008.

[2] "Maxon DC motor and maxon EC motor: Key information," May 2008. [Online]. Available: https://shop.maxonmotor. com/maxon/assets_external/Katalog_neu/Downloads/Katalog_PDF/ maxon_ec_motor/wichgtiges_dc_ec_motoren_08_036-043_e.pdf

[3] Z. Liu, D. Howe, P. Mellor, and M. Jenkins, "Thermal analysis of permanent magnet machines," *Electrical Machines and Drives, 1993. Sixth International Conference on*, pp. 359 – 364, Dec 1992.

[4] Y. Bertin, E. Videcoq, S. Thieblin, and D. Petit, "Thermal behavior of an electrical motor through a reduced model," *Energy Conversion, IEEE Transaction on*, vol. 15, no. 2, pp. 129 – 134, Jun 2000.

[5] C. Jang, J. Y. Kim, Y. J. Kim, and J. O. Kim, "Heat transfer analysis and simplified thermal resistance modeling of linear motor driven stages for SMT applications," *Components and Packaging Technologies, IEEE Transactions on*, vol. 26, no. 3, pp. 532 – 540, Sep 2003.

[6] J. Fiene, K. Kuchenbecker, and G. Niemeyer, "Event-based haptic tapping with grip force compensation," *Haptic Interfaces for Virtual Environment and Teleoperator Systems, 2006 14th Symposium on*, pp. 117 – 123, Feb 2006.

[7] D. C. Giancoli, *Physics for Scientists and Engineers*. Prentice Hall, Jan 2000.

[8] D. Staton, A. Boglietti, and A. Cavagnino, "Solving the more difficult aspects of electric motor thermal analysis," *Electric Machines and Drives Conference, 2003. IEMDC'03. IEEE International*, vol. 2, pp. 747 – 755 vol.2, May 2003.

[9] "Maxon motor catalog: A-max-26 7w," p. 117, May 2008. [Online]. Available: https://shop.maxonmotor.com/ maxon/assets_external/Katalog_neu/Downloads/Katalog_PDF/ maxon_dc_motor/A-max-programm/A-max-26_110181_08_117_e.pdf

[10] D. A. Paice, "Motor thermal protection by continuous monitoring of winding resistance," *Industrial Electronics and Control Instrumentation, IEEE Transactions on*, vol. IECI-27, no. 3, pp. 137 – 141, Aug 1980.

[11] J. Fraden, *Handbook of Modern Sensors: Physics, Designs, and Applications*. Springer Science+Business Media, LLC, Jan 2004.

[12] S. Kusui and T. Nagai, "An electronic integrating heat meter," *Instrumentation and Measurement, IEEE Transactions on*, vol. 39, no. 5, pp. 785 – 789, Oct 1990.

[13] P. Lang, "Calculating heat transfer across small gas-filled gaps," *Nucleonics*, Jan 1962.

[14] "Maxon motor catalog: RE-16 4.5w," p. 76, May 2008. [Online]. Available: https://shop.maxonmotor.com/ maxon/assets_external/Katalog_neu/Downloads/Katalog_PDF/ maxon_dc_motor/RE-programm/RE-16_118725_08_076_e.pdf

[15] A. Dagg, "Gaits in mammals," *Mammal Review*, vol. 3, no. 4, pp. 135 – 154, 1973.

[16] E. R. Pinch, *Optimal Control and the Calculus of Variations*. Oxford University Press, Jan 1993.

[17] S. Kim, M. Spenko, S. Trujillo, B. Heyneman, D. Santos, and M. Cutkosky, "Smooth vertical surface climbing with directional adhesion," *Robotics, IEEE Transactions on*, vol. 24, no. 1, pp. 65 – 74, Feb 2008.